AKADÉMIAI KIADÓ

Central European Geology

65 (2022) 2, 111–121

DOI: 10.1556/24.2022.00124

RESEARCH ARTICLE

Fully spherical 3D datasets on sedimentary particles: Fast measurement and evaluation

ESZTER FEHÉR[1,2*], BALÁZS HAVASI-TÓTH[1,3] and BALÁZS LUDMÁNY[1,4]

[1] MTA-BME Morphodynamics Research Group, Budapest, Hungary

[2] Department of Morphology and Geometric Modeling, Budapest University of Technology and Economics, Budapest, Hungary

[3] Department of Fluid Mechanics, Budapest University of Technology and Economics, Budapest, Hungary

[4] Department of Control Engineering and Information Technology, Budapest University of Technology and Economics, Budapest, Hungary

Received: January 26, 2022 • Accepted: June 13, 2022
Published online: September 14, 2022

ABSTRACT

Recently it became increasingly evident that the statistical distributions of size and shape descriptors of sedimentary particles reveal crucial information on their evolution and may even carry the fingerprints of their provenance as fragments. However, to unlock this trove of information, measurement of traditional geophysical shape descriptors (mostly detectable on 2D projections) is not sufficient; fully spherical 3D imaging and mathematical algorithms suitable to extract new types of inherently 3D shape descriptors are necessary. Available 3D imaging technologies force users to choose either speed or full sphericity. Only partial morphological information can be extracted in the absence of the latter (e.g., LIDAR imaging). In the case of fully spherical imaging, speed was proved to be prohibitive for obtaining meaningful statistical samples, and inherently 3D shape descriptors were not extracted. Here we present a new method by complementing a commercial, portable 3D scanner with simple hardware to quickly obtain fully spherical 3D datasets from large collections of sedimentary particles. We also present software for the automated extraction of 3D shapes and automated measurement of inherently 3D-shape properties. This technique allows for examining large samples without the need for transportation or storage of the samples, and it may also facilitate the collaboration of geographically distant research groups. We validated our software on a large sample of pebbles by comparing previously hand-measured parameters with the results of automated shape analysis. We also tested our hardware and software tools on a large pebble sample in Kawakawa Bay, New Zealand.

KEYWORDS

3D scanning, automated shape extraction, automated shape evaluation, full sphericity, morphology

INTRODUCTION

Since at least the seminal paper of Zingg (1935) it is widely recognized that the shape of sedimentary particles carries highly relevant information based on which essential parts of their evolutionary history may be reconstructed. Theoretical results and mathematical models of abrasion processes show that analysis of the shape of rocks may answer questions related to their place of origin and travel distance, and it can also reveal details of the abrasive forces that contributed to the final geometry (Szabó et al., 2015; Domokos et al., 2015, 2017; Novák-Szabó et al., 2018). On the one hand, this long tradition permits the comparison of datasets measured decades apart; on the other hand, it also narrows the list of shape descriptors, which scientists tend to prefer, for the very reason of comparability. It may be related to this long tradition and the desire to obtain results comparable with the literature,

*Corresponding author: Department of Morphology and Geometric Modeling, Budapest University of Technology and Economics, K220, Műegyetem rkp. 1–3., H-1111 Budapest, Hungary. E-mail: feher.eszter@epk.bme.hu

that shape measurement is almost exclusively restricted to classical, two-dimensional shape descriptors, such as axis ratios, roundness (Wentworth, 1923; Wolman, 1954) and descriptors derived from these quantities. Axis ratios are c/a and b/a, where a is the longest axis, b is the second longest axis in the perpendicular direction and c is the third longest axis perpendicular to the other two directions. The roundness is the isoperimetric ratio of the largest planar projection of the object

$$I_p = \frac{C_p^2}{4\pi A_p}, \quad (1)$$

where C_p is the circumference and A_p is the area of the planar projection, and it expresses how close the projection is to a circle. Traditional measurement techniques often incorporate personal factors or rely on the verbal characterization of the shape (Wentworth, 1923; Boggs, 2001) to approximate these values.

However, restricting the measurements to two-dimensional properties results in the loss of information regarding the total shape. The roundness might tell that the largest planar projection is close to a circle, but the shape can still be far from being a sphere. Although the three-dimensional isoperimetric ratio

$$I = \frac{A^3}{36\pi V^2}, \quad (2)$$

expresses how close the shape is to a sphere more accurately by implying the volume V and surface area A of the object, the measurement of the latter is not straightforward. The number of stable (S) and unstable (U) mechanical equilibria of a particle as a shape descriptor gained significant attention recently (Domokos et al., 2009; Miller et al., 2014; Domokos et al., 2015; Novák-Szabó et al., 2018). They express the number of resting points of an object, and they are three-dimensional properties in the sense that they cannot be recovered from planar projections of the object. Lying on a stable equilibrium point, the object responds to small perturbations by returning to its original position. On the contrary, any small perturbation of an object lying on an unstable equilibrium point is amplified and the object rolls away from its original position. As a result, S and U can be counted easily by hand, and they also have a rich mathematical literature (Grayson, 1987; Domokos et al., 2015; Domokos and Lángi, 2019). Based on the latter, we can make predictions for the evolution of S and U under abrasion processes, and therefore they can be used to understand the history of a pebble. One of the most widespread mathematical models of abrasion is proposed by Firey (1974), in which the abrasion depends on the curvature of the object. We know from Domokos (2015) that the number of balance points of the pebbles is monotonic under curvature-dependent mathematical models of abrasion. The qualitative behavior of these parameters is insensitive to both the model parameters and the measurement errors. However, the inaccuracy of the hand measurements is larger for U than for S, and it is a characteristic of the experimenter (Domokos et al., 2012a, b). As a result, the accuracy of the measurements can be increased by carrying out all the measurements by one person or by evaluating the particles automatically by computer software.

Previously, the technical complexity and impracticality of three-dimensional measurements resulted in the compromise of restricting the analysis to two-dimensional parameters (Hayakawa and Oguchi, 2005; Roussillon et al., 2009). We aimed to overcome the technical problems of three-dimensional measurements by offering a method that quickly creates a fully spherical three-dimensional scan of the particle and analyses its shape automatically. Moreover, it is also beneficial to completely replace hand measurements – even the two-dimensional ones – with automated shape analysis to avoid personal bias and speed up the data acquisition. Recording and storing three-dimensional geometries have numerous advantages in terms of collaboration with other researchers or groups and even later investigations of novel theories of the same dataset. Furthermore, in some special cases, such as abrasion experiments in a flume (Attal and Lavé, 2009) or a rotating drum (Imre et al., 2010), and pebble transport field experiments (Grottoli et al., 2019), the shape of the specimen changes during the experiment. Capturing the change requires measuring the shape properties at multiple different stages of the experiment.

The most precise way to record the shape is to create a fully spherical three-dimensional scanning which can be later used to extract any two- or three-dimensional shape parameters. Recently, several works appeared aiming to reduce subjectivity by automatically calculating shape properties from 2D digital images of the particles (Roussillon et al., 2009; Durian et al., 2007; Cassel et al., 2018; Cheng et al., 2018), 3D laser scanning (Hayakawa and Oguchi, 2005; Anochie-Boateng et al., 2013) or X-ray CT (Deiros Quintanilla et al., 2019). Development in sensors and 3D cameras induced a technological revolution in shape detection in many fields, from the poultry industry (Chan et al., 2018) to ballast in railway track structures (Anochie-Boateng et al., 2013). 3D scanning was successfully applied in geology for the analysis of rocks. Among the obvious advantages of these techniques, most papers reported some drawbacks compared to hand measurements. The workflow usually starts with collecting the samples and transporting them to the laboratory to scan. The scanning involves capturing the object in different positions and merging the resulting surfaces in a postprocessing step to obtain the full 3D shape. In the case of former geometry reconstruction techniques, a series of photos or partial scans need to be taken of the pebbles placed on flat surfaces from different angles before the assembly of the final geometry. Unfortunately, the merging procedure is not straightforward and usually has to be done manually, which is often extremely time-consuming due to removing the undesired surfaces attached to the pebble geometry. Moreover, most handheld scanners often suffer from issues when recording small objects and easily lose track of pebbles under a certain size. There are numerous options for 3D scanning, and most of them

require a well-prepared laboratory environment. Professional scanners are usually limited in portability, relatively expensive, and developed for scanning one object at a time, aiming for high precision. There exist techniques aiming at portability that do not require costly devices. Such a method is the surface reconstruction from photo sequences taken from different directions of the object, which is a technique unsuitable for capturing hundreds of specimens. There is a trade-off between portability and the amount of work needed to obtain the final image. Obtaining fully spherical scans of the objects is relatively slow, and taking the postprocessing into account, it can take weeks to capture a statistically significant number of specimens.

The purpose of our work is twofold. Firstly, we introduce a new workflow of 3D scanning that solves many of the issues regarding the 3D analysis of rocks and allows for the fast and automated extraction of 3D-shape data of large sets of samples. Secondly, we combine the technique with our algorithm to analyze a point cloud captured from the object and computationally determine its inherently three-dimensional shape properties. Our method is based on a portable scanner Structure Sensor Mark I, and software built on a recently published algorithm (Ludmány and Domokos, 2018) to analyze the point cloud. We utilize the fact that the algorithm works with the convex envelope of the point cloud and a polygonal approximation. As a result, it is unnecessary to aim for extremely high precision during the scanning, and the quality of simple portable scanners is satisfactory. The main advantage of our technique is that there is no need to transport the samples and store them for further analysis in the laboratory; hundreds of them can be captured in a few days near their origin, and the resulting 3D images can be analyzed later by the software. Such a technique could advocate data sharing and collaboration between experimental and theoretical groups. The structure of our paper is the following: in Section "Methodology", we introduce the scanning process and the remarkably short postprocessing resulting in the 3D point cloud, and the software carrying out the shape analysis is described in detail. Section "Benchmark" is devoted to validating the technique on a reference set of specimens and comparing hand-measured data to the computed shape properties. In Section "Field study", we illustrate the robustness of the method in a field-measurements at Kawakawa Bay, New Zealand. Finally, we summarize our results in Section "Conclusions".

METHODOLOGY

Our approach consists of a scanning technique that allows for the fully spherical scanning of a large set of samples and a postprocessing step to bulk evaluate their shape properties (Fig. 1).

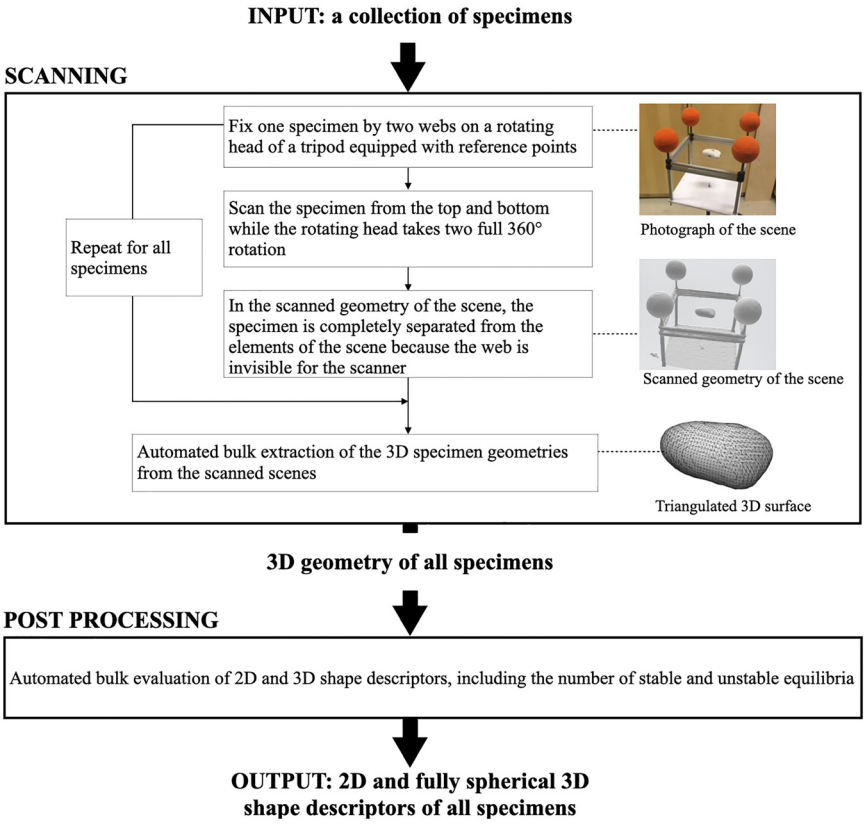

Fig. 1. Overview of the approach to obtain fully spherical geometry and carry out the automated shape analysis. The scanning process consists of scanning the sample lying on an invisible web and its environment, followed by the automated extraction of the shape. In the postprocessing step, we extract the 3D shape descriptors by analyzing the convex hull of the surface

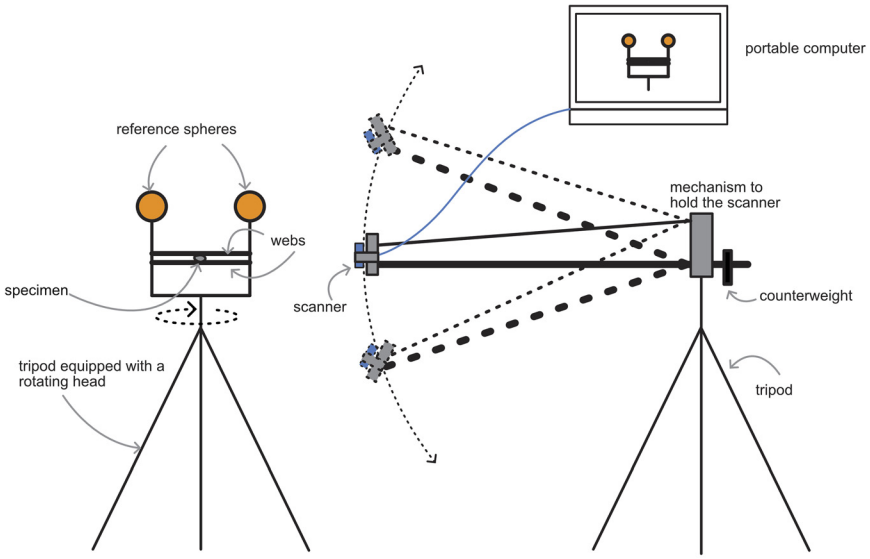

Fig. 2. Side view of the hardware layout. The left tripod is equipped with a rotating head and two webs invisible for the scanner to fix the specimen. Reference spheres enrich the scene to support the scanner's orientation. The right tripod carries a crane mechanism to hold the scanner, which can move up and down along a curved path so that it always faces the scene. A portable computer is connected to the scanner to record the geometry. A full 360° rotation of the specimen is allowed by the rotating head on the left tripod, while the scanner can move up and down while not losing sight of the specimen. The combination of these two motions allows for a fully spherical scanning

Hardware

The hardware layout consists of one tripod equipped with a rotating head and webs for the sample and another tripod with a crane mechanism to hold the scanner (Figs 2–3).

We aimed at elaborating a scanning technique that allows the uninterrupted scanning of pebbles resulting in a seamless geometry without any manual postprocessing. The sample should be fixed so that the entire surface is visible; hence, there is no need to scan different sides separately and merge at the end. One of the most crucial questions is how the pebble should be fixed in space without even a small part of its surface being covered by the holder. To overcome this problem, we constructed a holder of two 0.25 x 0.25 m frames with tight webs (Fig. 3). As long as the strings forming the webs are thin enough to be invisible to the scanner device, the frames manage to hold the pebble stationary, leaving plenty of space for the observer to scan each side. The frames are placed on a tripod equipped with a rotating head. The scanner we used does not have a built-in gyroscope or accelerometer, and it computes its relative spatial position and orientation merely based on the recorded three-dimensional point cloud. Therefore, to facilitate a robust and accurate orientation, we placed four spherical foam balls over the frames providing sufficiently large reference surfaces for the orientation regardless of the pebble size. The domain is automatically attached to the rotating frames without global reference points. Note that, in the case of newer scanners that might be equipped with an Inertial Measurement Unit, these reference points are not necessary.

Fig. 3. Layout of the hardware that allows for a fully spherical scanning. Two webs carry the specimen, and a crane mechanism holds the scanner and ensures smooth motion without losing sight of the object

We designed the assembly to be rotated smoothly on a tripod. The scanner is fixed on a tripod equipped with a camera crane. It is crucial for the scanner never to lose track of the pebble during the scanning process. Hence the crane is designed to move the scanner so that the sample always remains in the center of the view regardless of the crane angle. As Fig. 4 shows, the scanner defines a scanning domain in which it generates the geometry based on the distance field, while everything outside the domain is completely ignored. After the scanning process is initiated, it is essential for the successful scanning to never let the domain out of sight of the scanner.

After fixing the pebble in the frame, the scanning can be performed in one continuous session using the Structure Sensor Mark I scanner. The scanning starts at the upper

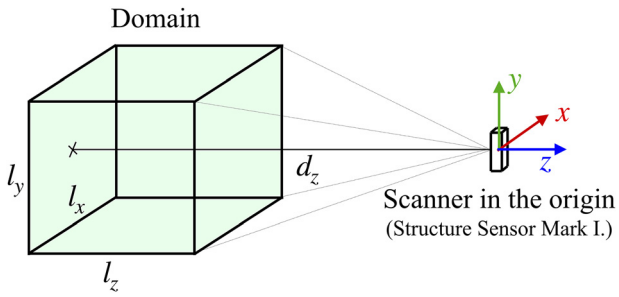

Fig. 4. The position and dimensions of the scanning domain; $d_z = 0:8\ m$, $l_x = l_y = l_z = 0.5\ m$

position of the crane, and after a full 360-degree rotation of the sample, the crane moves downwards, which is followed by a second 360-degree turn of the sample. This method ensures that every side of the sample is captured. The scanner is connected to a computer running Skanect Pro, recording the geometry.

Finally, the geometry containing the sample and its surroundings with the frame of the web and the reference spheres are exported to stereolithography format. Since the web remains invisible, the pebble geometry is independent of its surroundings, and the pebble can be easily extracted by a suitable algorithm for automation. With this procedure, one pebble can be scanned in under two minutes. The new scanning technique is compared to the existing methods in Table 1. Although the proposed method for fully spherical scanning defeats existing methods in terms of portability, speed, and price, portable scanners are expected to create point clouds of lower quality for small specimen sizes compared to a fixed laser scanner or CT, X-ray technologies. We will show in Section "Benchmark" that the size limit of a sample for Structure Sensor Mark I. was 1,000 mm^3. A video demonstration of the new method is available at Fehér et al., (2020).

Software

Although there exist approaches to analyze a 3D scanned geometry (Hayakawa and Oguchi, 2005; Deiros Quintanilla et al., 2019), they are unable to extract the number of stable and unstable equilibrium points. Our software is based on the algorithm of Ludmány and Domokos (2018) and available in Ludmány (2020b). It aims to automatically measure traditional three-dimensional shape properties and the number of equilibrium points.

The scanning process results in a triangulated point cloud, a polyhedral approximation of the surface. Since the number of equilibrium points is defined for the convex hull of the body, the faces of the input files are ignored, and a triangulated convex hull of the points is constructed right away (Fig. 5). We consider the homogeneous body bounded by the convex hull with the origin at its center of mass. We define the boundary surface in spherical coordinates $r(\vartheta, \varphi)$, where r is the radial distance of the boundary point measured from the reference point, ϑ and φ are the polar and azimuthal angles, respectively. The equilibrium points are the extreme values of the radial distance function of the convex hull.

It was shown by Domokos et al. (2012 a, b) that a polyhedral approximation of a surface results in artificial equilibrium points. We overcome this problem by introducing a new definition of the equilibrium points on the contour representation of the triangulated surface. The algorithm calculates level sets of the radial distance function from the reference point to the convex hull and represents the body by M contour lines enclosing points lying at least at a distance s_i, where i = 1,…,M. The reference point is the centroid of the convex hull by default. The equilibrium points are represented by contour lines that do not contain contour lines with an area larger than ρ percent of the total surface area. Parameters M and ρ provide smoothing of the surface to avoid the effects of the polyhedral approximation of the body and the imperfections coming from the scanning process. Increasing ρ and decreasing M both increase the smoothness of the surface in terms of the equilibrium points. Both M and ρ are input parameters of the algorithm.

The center of mass of the real object can differ from the centroid of its convex hull for concave shapes or inhomogeneous objects. The software can take multiple reference points to consider the uncertainties. It takes m number of reference points distributed uniformly inside a sphere of radius R around the centroid and calculates the number of stable and unstable points for each one. It is possible to calculate the minimum, maximum, or average of these values, which we refer to as the aggregation method. Apart from the number of equilibrium points, the algorithm calculates multiple two- and three-dimensional geometrical properties of the convex hull. Instead of calculating the isoperimetric ratios defined in the introduction, the software calculates their normalized inverse, which lies between 0 and 1. If a two-dimensional shape is close to a circle, the normalized inverse of its isoperimetric ratio becomes close

Table 1. Comparison of the existing techniques and the proposed method in terms of portability, recording and postprocessing speed, and price

Technique	Portability	Recording speed	Postprocessing speed	Price	References
fixed 3D scanner	–	slow (30 min)	slow (30 min)	expensive	Hayakawa and Oguchi (2005), Anochie-Boateng et al. (2013)
3D from 2D photos	x	slow (40–200 images)	slow (1 h)	cheap	Tomasi and Kanade (1992)
CT, X-ray	–	slow (7 particle/day)	fast	very expensive	Deiros Quintanilla et al. (2019)
proposed method	x	fast (2 min)	fast (1 min)	cheap	

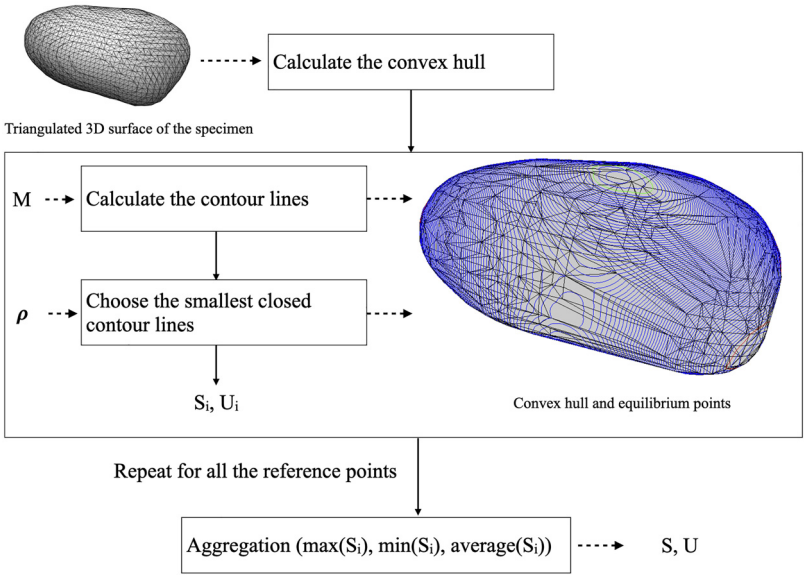

Fig. 5. Algorithm to calculate the number of equilibrium points from a three-dimensional geometry. The convex hull of the pebble geometry is represented by black lines. The algorithm calculates the contour lines (blue curves) considering the ith reference point. The stable and unstable equilibrium points lie inside the green and red contour lines, respectively. Counting these contour lines results in S_i and U_i. The steps are repeated for all reference points and an aggregation method is used to find the final S and U

to 1. Similarly, when the normalized inverse of the three-dimensional isoperimetric ratio is close to 1, it means that the shape is close to the sphere. The two-dimensional data are calculated for the planar projection of the convex hull, which has the largest possible area. The two-dimensional outputs are the following:

- circumference (C_p) and area (A_p) of the planar projection
- the longest axis (a_p), and the second longest (b_p) in the perpendicular direction of the planar projection
- normalized inverse of the two-dimensional isoperimetric ratio of the planar projection $\left(\overline{I}_p = \frac{4\pi A_p}{C_p^2}\right)$
- normalized inverse of the two-dimensional isoperimetric ratio of an ellipse with axes a_p and b_p $\left(\overline{I}_{pe} = \frac{4\pi a_p b_p \pi}{C_{pe}}\right)$, where C_{pe} is the circumference of the ellipse

Three-dimensional outputs:

- the number of stable (S) and unstable (U) equilibrium points
- surface area (A) and volume (V) of the convex hull
- longest (a), second-longest perpendicular to the longest (b) and third longest axis perpendicular to the other two (c) and their ratios (c/a, b/a)
- normalized inverse of the three-dimensional isoperimetric ratio of the convex hull $\left(\overline{I} = \frac{36\pi V^2}{A^3}\right)$
- normalized inverse of the three-dimensional isoperimetric ratio of an ellipsoid with axes a, b, c ($\overline{I}_e = \frac{36\pi V_e^2}{A_e^3}$, where A_e and V_e are the surface area and the volume of the ellipsoid, respectively).

There are two modes of operation: the user can either open a single file or a batch of files. In the first case, the convex hull is displayed in a 3D viewer, and the equilibrium points found by the algorithm are visualized. This allows for the rapid and straightforward comparison of the scanned geometry with the real object. The second mode is a bulk evaluation of multiple files using predefined values of the input parameters M, ρ, m, R in a batch file (in CSV format). In the case of m = R = 0 the reference point is the centroid; otherwise, an aggregation method is also required. The results can be saved in CSV format, and the statistical analysis can be carried out separately. The computation is parallelized, and depending on the parameters and the number of pebbles, it takes only a few minutes. The computer program presented here is merely a user-friendly graphical interface on top of the algorithm, which is separated in a function library available in Ludmány (2020a). This technology can be easily integrated into any other application.

BENCHMARK

We fitted the input parameters of the software to hand-measured data of 367 pebbles and fragments from various locations, including different rock types and colors. From the output parameters of the algorithm listed in Section "Software", we restricted the benchmark test on a, b, c, S, U, which can be measured reliably. One person carried out the hand measurements under laboratory conditions for consistency. We scanned the specimens with the method described in Section "Hardware" and evaluated the geometries with the algorithm using different parameter combinations of M, ρ, m, R. Firstly the a, b, c values were used to check the scanning quality since they are independent of the input parameters and cannot be improved. Since the

uncertainty in the hand measurement of U is larger than for S, we fitted the input parameters to the measured number of stable equilibrium points and expected a higher difference for U. We defined two error norms:

$$\bar{e}_S = \frac{1}{N}\sum_{i=1}^{N}\frac{\left|S_i^m - S_i^c\right|}{S_i^m}, \tag{3}$$

$$\bar{e}_U = \frac{1}{N}\sum_{i=1}^{N}\frac{\left|U_i^m - U_i^c\right|}{U_i^m}, \tag{4}$$

$$e_{\overline{S}} = \frac{\left|\sum_{i=1}^{N} S_i^m - \sum_{i=1}^{N} S_i^c\right|}{\sum_{i=1}^{N} S_i^m}, \tag{5}$$

$$e_{\overline{U}} = \frac{\left|\sum_{i=1}^{N} U_i^m - \sum_{i=1}^{N} U_i^c\right|}{\sum_{i=1}^{N} U_i^m}, \tag{6}$$

where e_S, e_U are the average of the errors, sample by sample, and $e_{\overline{S}}$, $e_{\overline{U}}$ are the errors of the average for a set of N pebbles. For statistical analysis, the average error is more relevant.

Six different sets of pebbles (A1, C1, K1, N1, TA1, T2) and 1 set of fragments (F) were analyzed and evaluated using the same parameter combinations. By comparing a, b, c, the limits of the scanner were also tested: samples that were too small resulted in significant differences in a, b, c; as a result, we limited the volume to V = 1,000 mm^3. The size of the samples ranged from 1,000 to 21,000 mm^3. The best fit of the parameters was M = 200, ρ = 0.05, m = 10, R = 0.001, which resulted in good agreement between the measurements and computations for pebbles.

The measured axis lengths are plotted against their computed values in the histograms of Fig. 6. Based on the definition of the axis lengths (see Section "Software"), we expect the best agreement for the longest axis length (a) and the worst for the third axis length (c), which is relatively hard to find by hand measurement. The spread is larger in Fig. 6 c) than in Fig. 6 a) in agreement with our expectations.

Table 2 summarizes the S, U data and Fig. 7 shows the error of the averages for each set. Note that S and U are integral numbers, so the error can be relatively high. Due to the averaging evaluation, we expect that the method will not detect extremities, e.g., it would not detect monostatic bodies. However, due to the uncertainty in the exact location of the centroid, the consideration of multiple reference points is inevitable. As we can see in Fig. 7, the error is relatively high in the case of fragments (set F), which can be attributed to the precision of the scanner. According to the manufacturer, the precision is 0.5 mm in the best possible case. The scanner did not capture the edges of the fragments appropriately, leading to a loss of equilibrium points. Nevertheless, portable scanners are continuously progressing, and we expect better agreement in the future.

FIELD STUDY

We demonstrate the robustness of the technique on beach pebbles from Kawakawa Bay, New Zealand (Fig. 8).

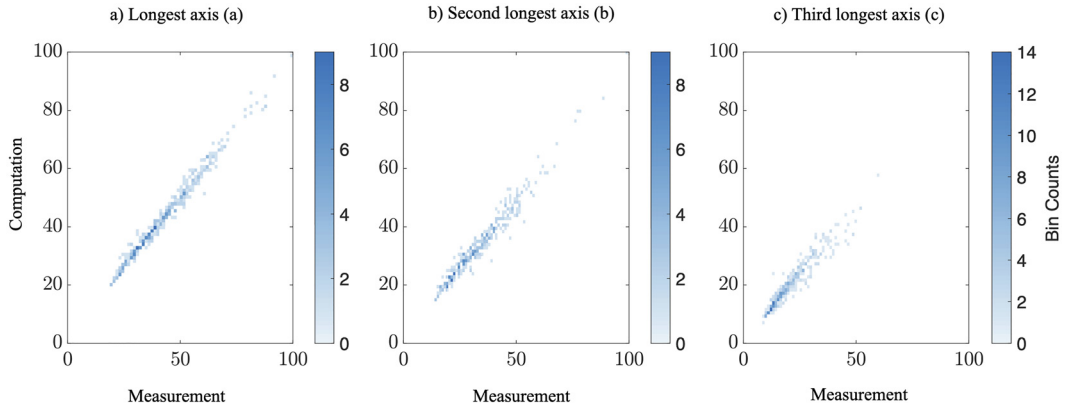

Fig. 6. Computed axis lengths against their measured values. The color shows the number of pebbles lying in the specified bin of the 2D histogram. The comparison includes all 367 pebbles and fragments. a) b)

Table 2. The computed and measured averages of the S and U values and the errors in percentage. Std is the standard deviation of the error for each individual pebble and N is the number of specimens in the set

sample	$\overline{S}^c$	$\overline{S}^m$	std(S)	$\overline{U}^c$	$\overline{U}^m$	std(U)	$\bar{e}_S$[%]	$\bar{e}_U$[%]	$e_{\overline{S}}$[%]	$e_{\overline{U}}$[%]	N
A1	4.26	4.63	0.98649	3.35	3.94	0.73835	22.98	27.51	7.84	12.7	16
C1	3.67	4.17	0.76444	3.4	3.26	0.61465	22.99	15.01	11.89	3.37	42
F	3.91	4.81	1.0982	5.36	5.62	1.0069	24.03	21.47	18.82	5.49	53
K1	2.75	2.35	0.83028	3.19	2.77	1.1825	26.75	27.08	16.81	17.79	48
N1	2.49	2.5	0.60763	2.66	2.68	0.6995	13.1	13.28	0.21	0.84	76
T2	3.78	3.98	1.0473	3.24	3.18	0.70482	24.84	26.37	4.97	1.68	45
TA1	2.9	3.88	0.79303	3.48	3.82	0.74364	25.2	16.34	25.21	8.74	49

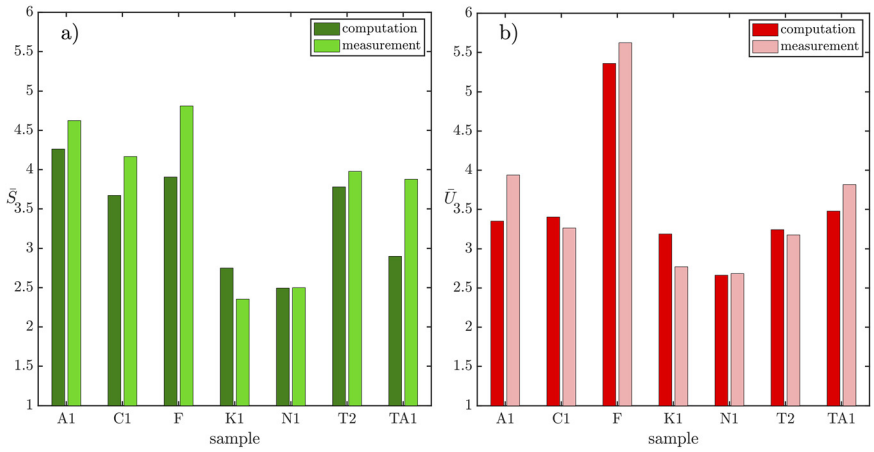

Fig. 7. Average of the computed and measured number of stable and unstable equilibrium points for seven sets of samples using the best parameter combinations. a) Comparison of $\overline{S}$. b) Comparison of $\overline{U}$

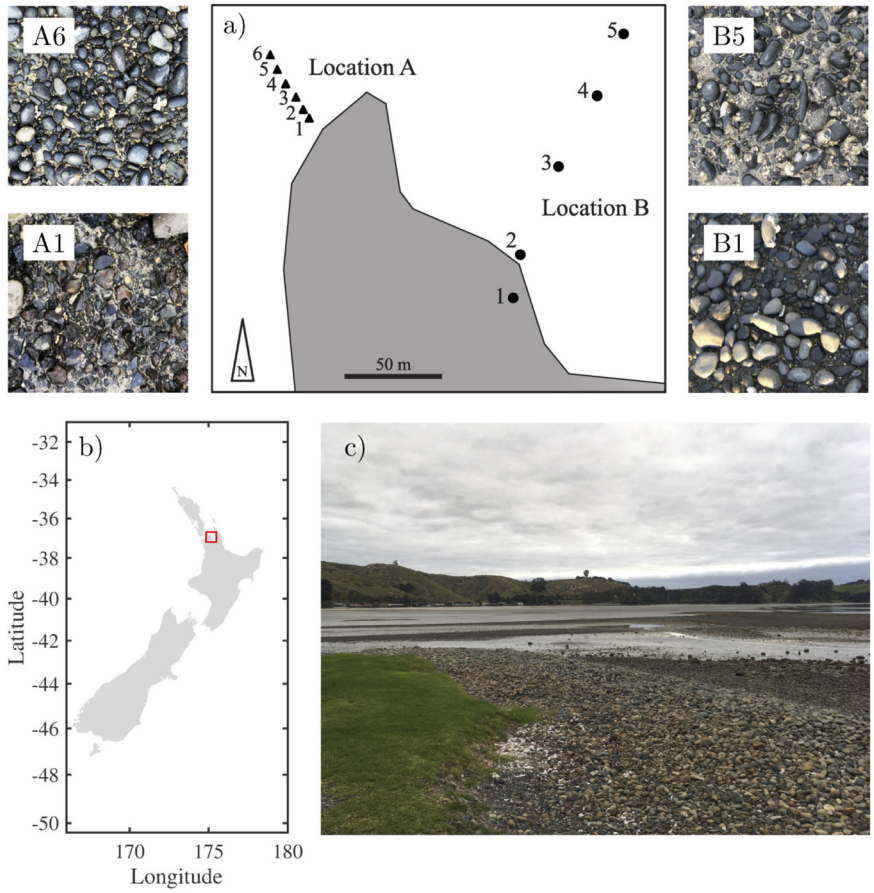

Fig. 8. Kawakawa Bay, New Zealand. a) Location A and B. b) Map of New Zealand with Kawakawa Bay highlighted by a red square. c) A photograph of Kawakawa Bay at Location B

We performed the technique of Wolman (1954) for collecting 20–40 randomly chosen pebbles at each location. Firstly, we chose two locations and appointed measurement points lying at approximately equal distances along a line. A measurement point represented a line segment parallel to the coastline. The collecting person was moving from side to side, and the collecting process stopped when a satisfactory number of pebbles was obtained. We scanned the collected samples with the proposed method and evaluated the geometries using the input parameters determined in Section "Benchmark" (Fig. 9 and 10).

Location A consisted of six measurement points lying approximately 8 m away from each other in the direction perpendicular to the coastline. The pebbles were slightly

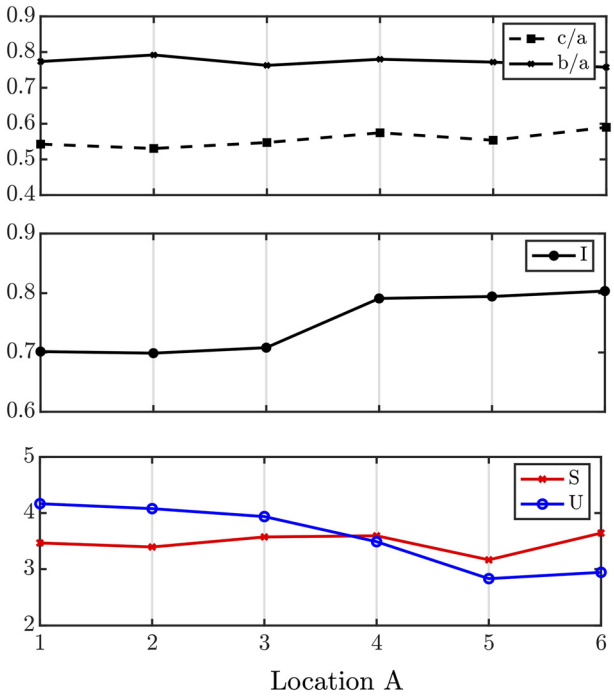

Fig. 9. Shape properties were evaluated on the scanned geometries of the samples collected from six measurement points of Location A. Location A1 is the closest to the coast. The results show that from locations A1 to A6, the particles gradually change their shape. The number of unstable equilibrium points decreases, the isoperimetric ratio increases, and the other parameters stay approximately constant

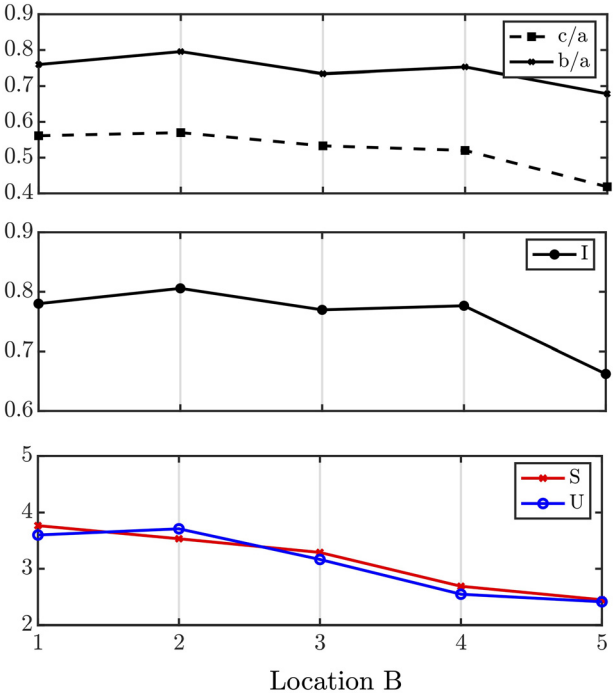

Fig. 10. Shape properties were evaluated on the scanned geometries of the samples collected from five measurement points of location B. The decrease in all the measured shape properties shows that. moving farther from the coast, the particles become elongated

embedded in the sand. We marked some of them, and during 3–4 sunny days, most of the marked pebbles maintained their positions. We found fragments at location A1 near the coast and rounded pebbles at location A6, but there was no visible difference between them in terms of size distribution. We conjectured that the particles along Location A have the same origin, but those that are lying farther from the coast have small sharp edges and corners eroded. Otherwise, we expected no significant difference between rocks along the line. The analysis supported our expectations. The aspect ratios c/a, b/a, and S stayed approximately constant along the line, but U decreased, and I increased (Fig. 9). The number of samples was 20–30 at each location; the size distribution was between 11,500 and 108,000 mm^3.

Location B consisted of five points lying approximately 38 m away from each other. The path was also perpendicular to the coastline. Subjective comparison of the pebbles of locations B1 and B5 suggested that the latter are more abraded. At location B5, the number of elongated pebbles seemed to be significantly higher compared to location B1 based on visual inspection. The scanning analysis proved this assumption. Both the aspect ratios decreased, meaning that the two sizes of the pebbles decreased more than the longest size, leading to an elongated geometry. Subsequently, I also decreased with S and U decreasing (Fig.10). The number of specimens was 15–30, and the size distribution was between 5,000 and 170,000 mm^3.

Although the benchmark test in Section "Benchmark" showed that using the Structure Sensor Mark I, sharp edges cannot be recorded and results in a slightly decreased S and U; using this technique, we managed to capture the gradual changes at both locations. We collected and scanned approximately 400 pebbles and fragments in three days without the need to transport the pebbles to the laboratory. Moreover, the dataset is available for further analysis.

CONCLUSIONS

A new, rapid scanning technique was introduced to create a fully spherical scan of pebbles and fragments. We also presented our software to evaluate the shape properties of the scanned objects and replace hand measurements.

Introducing portable scanners to geologic applications makes it unnecessary to transport the collected samples to the laboratory. Moreover, the postprocessing takes only a few minutes using the suggested setup, and it can be easily automated. Two- and three-dimensional shape properties, such as the axis ratios, the inverse of the isoperimetric ratios, and the number of static equilibria, are evaluated using the convex hull of the point cloud representing the surface with contour lines. The technique is proved to be an excellent alternative to hand measurements. We expect accelerated development on the hardware side. Structure Sensor Pro is already available, and the compatible Skanect Pro version is on the go, extending the range of scannable pebble sizes and providing better precision for fragments. It is also expected that this measurement technique would encourage collaborations between international

groups through easy data sharing and storing. As the mathematical background of abrasion models and shape descriptors develops, new perspectives might appear to be examined on existing pebble geometries.

A possible extension of the method could be the scanning of multiple pebbles simultaneously. If the scanner is connected to an iPad, it can record the texture of the surface, e.g., an ID written on the sample. This way, the digitalized pebbles can be easily distinguished from each other. Structure Sensor Pro comes with a wide lens camera to record the texture without an iPad connection. Depending on the size of the pebble, it would be possible to scan 4–5 pebbles simultaneously, which could significantly reduce the overall scanning time.

Contribution

The steps of the 3D scanning process were developed by authors Balázs Havasi-Tóth and Eszter Fehér, and Balázs Ludmány developed the automated shape analysis algorithm. The benchmark tests and the field study were carried out by Balázs Havasi-Tóth and Eszter Fehér. All authors contributed to writing of the document and interpreting the results.

ACKNOWLEDGMENTS

The authors would like to thank Krisztián Halmos for carrying out the hand measurements and for helping with the 3D scanning; Gábor Domokos for the fruitful discussions and his help in the field study; Bernd Krauskopf for helping to find a location to test the method; Géza Tóth for helping to build the camera crane. This research, supported by the NKFIH Hungarian Research Fund Grant 134199 and by Grant BME FIKP-VÍZ by EMMI, is gratefully acknowledged. The research reported in this paper and carried out at BME has been supported by the NRDI Fund (TKP2020 NC, Grant No. BMENCS) based on the charter of bolster issued by the NRDI Office under the auspices of the Ministry for Innovation and Technology. This research is also part of project no. BME-NVA-02, implemented with the support provided by the Ministry of Innovation and Technology of Hungary from the National Research, Development and Innovation Fund, financed under the TKP2021 funding scheme.

REFERENCES

Anochie-Boateng, J.K., Komba, J.J., and Mvelase, G.M. (2013). Three-dimensional laser scanning technique to quantify aggregate and ballast shape properties. *Construction and Building Materials*, 43: 389–398, ISSN 0950-0618. https://doi.org/10.1016/j.conbuildmat.2013.02.062. URL: http://www.sciencedirect.com/science/article/pii/S0950061813001918.

Attal, M. and Lavé, J. (Dec. 2009). Pebble abrasion during fluvial transport: experimental results and implications for the evolution of the sediment load along rivers. *Journal of Geophysical Research: Earth Surface*, 14(F4). https://doi.org/10.1029/2009JF001328.

Boggs, S. (2001). *Principles of sedimentology and stratigraphy*. Prentice Hall. ISBN 9780130996961. URL: https://books.google.hu/books?id=L4LBQgAACAAJ.

Cassel, M., Piégay, H., Lavé, J., Vaudor, L., Sri, D.H., Budi, S.W., and Lavigne, F. (June 2018). Evaluating a 2d image-based computerized approach for measuring riverine pebble roundness. *Geomorphology*, 311: 143–157. https://doi.org/10.1016/j.geomorph.2018.03.020.

Chan, T., Lichti, D., Jahraus, A., Esfandiari, H., Lahamy, H., Steward, J., and Glanzer, M. (July 2018). An egg volume measurement system based on the microsoft kinect. *Sensors*, 18(8): 2454. https://doi.org/10.3390/s18082454.

Cheng, C., Li, S.-Y., and Peng, L. (Mar. 2018). A quantitative method of measuring roundness of outcrop gravels and its applications in the study of carbonate slope geometry. *Carbonates and Evaporites*, 33(4): 823–834. https://doi.org/10.1007/s13146-018-0446-x.

Deiros Quintanilla, G.C., Emeriault, F., Voivret, C., and Ferellec, J.-F. (Mar 2019). X-ray ct analysis of the evolution of ballast grain morphology along a micro-deval test: key role of the asperity scale. *Granular Matter*, 21(2): 30, ISSN 1434-7636, https://doi.org/10.1007/s10035-019-0881-y.

Domokos, G. (Apr. 2015). Monotonicity of spatial critical points evolving under curvature-driven flows. *Journal of Nonlinear Science*, 25(2): 247–275, ISSN 0938-8974. https://doi.org/10.1007/s00332-014-9228-3.

Domokos, G. and Lángi, Z. (2019). The isoperimetric quotient of a convex body decreases monotonically under the eikonal abrasion model. *Mathematika*, 65(1): 119–129. https://doi.org/10.1112/s0025579318000347.

Domokos, G., Sipos, A., Szabó, T., and Várkonyi, P. (Oct. 2009). Pebbles, shapes, and equilibria. *Mathematical Geosciences*, 42(1): 29–47. https://doi.org/10.1007/s11004-009-9250-4.

Domokos, G., Lángi, Z., and Szabó, T. (2012a). On the equilibria of finely discretized curves and surfaces. *Monatshefte für Mathematik*, 168(3): 321–345.

Domokos, G., Sipos, A.Á., and Szabó, T. (2012b). The mechanics of rocking stones: equilibria on separated scales. *Mathematical Geosciences*, 44(1): 71–89.

Domokos, G., Kun, F., Sipos, A.Á., and Szabó, T. (Mar. 2015). Universality of fragment shapes. *Scientific Reports*, 5(1). https://doi.org/10.1038/srep09147.

Domokos, G., Sipos, A.Á., Szabó, G.M., and Várkonyi, P.L. (dec 2017). Explaining the elongated shape of 'oumuamua by the eikonal abrasion model. *Research Notes of the AAS*, 1(1): 50. https://doi.org/10.3847/2515-5172/aaa12f.

Durian, D.J., Bideaud, H., Duringer, P., Schröder, A.P., and Marques, C.M. (Feb. 2007). Shape and erosion of pebbles. *Physical Review E*, 75(2). https://doi.org/10.1103/physreve.75.021301.

Fehér, E., Havasi-Tóth, B., and Ludmány, B. (2020). *A new workflow for the automated measurement of shape descriptors of rocks*. Budapest University of Technology and Economics, MTA-BME Morphodynamics Research Group. https://doi.org/10.5446/45980, Last accessed : 20 Mar. 2020.

Firey, W.J. (1974). Shapes of worn stones. *Mathematika*, 21(1): 1–11. https://doi.org/10.1112/S0025579300005714.

Grayson, M.A. (1987). The heat equation shrinks embedded plane curves to round points. *Journal of Differential Geometry*, 26(2): 285–314. https://doi.org/10.4310/jdg/1214441371.

Grottoli, E., Bertoni, D., Pozzebon, A., and Ciavola, P. (2019). Influence of particle shape on pebble transport in a mixed sand and gravel beach during low energy conditions: implications for nourishment projects. *Ocean and Coastal Management*, 169: 171–181, ISSN 0964-5691. https://doi.org/10.1016/j.ocecoaman.2018.12.014, URL: https://www.sciencedirect.com/science/article/pii/S0964569118305647.

Hayakawa, Y. and Oguchi, T. (July 2005). Evaluation of gravel sphericity and roundness based on surface-area measurement with a laser scanner. *Computers & Geosciences*, 31(6): 735–741. https://doi.org/10.1016/j.cageo.2005.01.004.

Imre, B., Laue, J., and Springman, S.M. (2010). Fractal fragmentation of rocks within sturzstroms: insight derived from physical experiments within the eth geotechnical drum centrifuge. *Granular Matter*, 12(3): 267–285. https://doi.org/10.1007/s10035-009-0163-1.

Ludmány, B. (Mar. 2020a). Library finding equilibria on 3d scanned pebbles. https://doi.org/10.5281/zenodo.3712785.

Ludmány, B. (Mar. 2020b). Frontend for library finding equilibria on 3D scanned pebbles. https://doi.org/10.5281/zenodo.3712787.

Ludmány, B. and Domokos, G. (2018). Identification of primary shape descriptors on 3d scanned particles. *Periodica Polytechnica Electrical Engineering and Computer Science*, 62(2): 59–64. https://doi.org/10.3311/PPee.12313, URL: https://pp.bme.hu/eecs/article/view/12313.

Miller, K.L., Szabó, T., Jerolmack, D.J., and Domokos, G. (2014). Quantifying the significance of abrasion and selective transport for downstream fluvial grain size evolution. *Journal of Geophysical Research: Earth Surface*, 119(11): 2412–2429. https://doi.org/10.1002/2014JF003156, URL, https://agupubs.onlinelibrary.wiley.com/doi/abs/10.1002/2014JF003156.

Novák-Szabó, T., Sipos, A.Á., Shaw, S., Bertoni, D., Pozzebon, A., Grottoli, E., Sarti, G., Ciavola, P., Domokos, G., and Jerolmack, D.J. (2018). Universal characteristics of particle shape evolution by bed-load chipping. *Science Advances*, 4(3). https://doi.org/10.1126/sciadv.aao4946, URL: https://advances.sciencemag.org/content/4/3/eaao4946.

Roussillon, T., Piégay, H., Sivignon, I., Tougne, L., and Lavigne, F. (Oct. 2009). Automatic computation of pebble roundness using digital imagery and discrete geometry. *Computers & Geosciences*, 35(10): 1992–2000. https://doi.org/10.1016/j.cageo.2009.01.013.

Szabó, T., Domokos, G., Grotzinger, J.P., and Jerolmack, D.J. (2015). Reconstructing the transport history of pebbles on mars. *Nature Communications*, 6(1): 8366. https://doi.org/10.1038/ncomms9366.

Tomasi, C. and Kanade, T. (Nov. 1992). Shape and motion from image streams under orthography: a factorization method. *International Journal of Computer Vision*, 9(2): 137–154. https://doi.org/10.1007/bf00129684.

Wentworth, C.K. (1923). A method of measuring and plotting the shapes of pebbles, Technical report. https://doi.org/10.3133/b730c.

Wolman, M.G. (1954). A method of sampling coarse river-bed material. *Transactions, American Geophysical Union*, 35(6): 951. https://doi.org/10.1029/tr035i006p00951.

Zingg, T. (1935). *Beitrag zur Schotteranalyse*, PhD thesis. ETH Zurich.

Appendix A

GPS coordinates.

The GPS coordinates of the measurement points of the field study are listed in Table A1 and Table A2.

Table A1: GPS coordinates of the measurement points at location A

ID	latitude	longitude
A1	36°56′49.1″S	175°09′51.0″E
A2	36°56′49.0″S	175°09′50.9″E
A3	36°56′48.7″S	175°09′50.7″E
A4	36°56′48.5″S	175°09′50.5″E
A5	36°56′48.3″S	175°09′50.3″E
A6	36°56′48.1″S	175°09′50.2″E

Table A2: GPS coordinates of the measurement points at location B

ID	latitude	longitude
B1	36°56′52.1″S	175°09′55.3″E
B2	36°56′51.4″S	175°09′55.4″E
B3	36°56′49.9″S	175°09′56.2″E
B4	36°56′48.7″S	175°09′57.0″E
B5	36°56′47.7″S	175°09′57.6″E